Environ Earth Sci (2016)75:537
DOI 10.1007/s12665-016-5419-6

ORIGINAL ARTICLE

Microstructure changes of red clay during its loss and leakage in the karst rocky desertification area

Yiqun Tang[1,2] · Kai Sun[1] · Xiaohui Zhang[1] · Jie Zhou[1,2] · Qi Yang[1] · Qi Liu[1,2]

Received: 15 April 2015 / Accepted: 30 January 2016

Abstract Karst rocky desertification is a unique type of desertification caused by unreasonable human activities in a vulnerable ecological environment. It has severely restrained the sustainable development of Southwest China. Chenqi village which is the studied area in this paper has suffered karst rocky desertification for decades. Red clay samples were collected from different sites around this village and analyzed through mercury intrusion porosimetry (MIP) and scanning electron microscope (SEM) tests. Then, the microstructure changes of soil during its loss and leakage were observed to study the impact of rainfall erosion and the mechanism of soil loss and leakage. The results demonstrate that the land use patterns can change the distribution of micro/small pores in soil. The shrub grass land, which is least exploited by human activities, has the largest volume of micro/small pores. Meanwhile, soil leakage can change the distribution of medium/large pores. The soil from surface (0–15 cm), which is deposited at the beginning of soil leakage, has the largest volume of medium/large pores. Pore surface fractural dimension is negatively correlated with human activity impact, and positively correlated with the distribution of micro and small pores. The microstructure can well represent different phases of soil loss and leakage as well as the soil breakage level.

✉ Yiqun Tang
tangyiqun2@tongji.edu.cn

[1] Department of Geotechnical Engineering, Tongji University, Shanghai 200092, People's Republic of China

[2] Key Laboratory of Geotechnical and Underground Engineering, Ministry of Education, Tongji University, Shanghai 200092, People's Republic of China

Keywords Karst rocky desertification · Loss and leakage · Land use and land cover change · Mercury intrusion porosimetry · Scanning electron microscope

Introduction

Karst topography, just like the edge of a desert, is considered as one of the main eco-sensitive zones on earth. It is extremely fragile to climate change and human activities (Yuan 1996). The karstification can induce land degradation, vegetation coverage loss, excess soil erosion, earthquakes, and the karst rocky desertification eventually (Wang et al. 2004). Karst rocky desertification has posed a great threat to many areas in Southwest China. The development of local society and economy as well as the living environment for residences are severely affected. To gain an insight into the effective ways to control soil erosion, this study focused on the basic and key issues of soil and water loss in the rocky desertification area. The study will contribute to the soil and water conservation and ecological restoration in this region.

Since karst rocky desertification (KRD) was noticed by scholars and engineers, a series of studies of soil erosion were carried out in different aspects. The studies include: the process and classification, causes and mechanisms, impact factors and its evolution, environmental response and destruction, prevention and control measures (Ellison 1947; Olson and Wischmeier 1963; Hu et al. 2003; Chen et al. 2009; Xiong et al. 2009; Yang et al. 2011, 2013, 2014; Jiang et al. 2014; Wang et al. 2014). Many scientific and technical methods were applied for the research on karst rocky desertification, such as geographical information system (Huang and Cai 2007), remote sensing (Kheir et al. 2008), experimental simulation (Tang et al. 2010; He et al. 2013),

Published online: 21 March 2016

hyperspectral image (Tobias et al. 2012) and computer model (Janža 2010). They have become effective tools to study soil erosion in karst rocky desertification areas.

In Guizhou province, China, large-scale surface runoff experimental stations were set up in the karst rocky desertification (KRD) area. The monitoring results revealed the influence of factors such as land use and rainfall condition on surface runoff erosion (Tang et al. 2009; Zhou et al. 2012). Although serious land degradation occurred in the tested regions, the test results show that merely a small amount of soil sediment was collected in the cutoff grooves within a certain period of time. This phenomenon indicates some other soil loss processes exist besides the surface runoff erosion.

The concept "soil and water loss" was first proposed by Trudgill and Clayton (1985). However, unlike the general soil and water loss, soil and water loss in karst areas refers to a more complicated process. The loose surface soil in karst areas is scoured, eroded and transported downstream by runoffs, and then leaks into the underground water system. The degree of soil loss in an area is closely related to the land use, land cover, falling gradient, and underground karst development (Li et al. 2001). In 2007, Zhang et al. proposed the important concept of "leakage loss of soil". He pointed out that the combined action of chemical weathering, mass wasting, and water erosion is the primary cause of soil loss in karst sloping area. The vertical movement of scoured soil along the karst channels is the primary mechanism of soil leakage in Southwest China.

The stability of surface soil, which is greatly affected by its microstructure, is a key factor to its anti-erosion capacity (Осипов 1985; Terzaghi et al. 1996; Ferro et al. 2012). Li et al. (2002) studied the classification of the microstructures of residual red clay through numerous SEM images. He pointed out that former researchers failed to take a full consideration of the forming conditions and deposit environment of soil. Wu (2004) and Wang (2008) found the connections between the LUCC (Land use and land cover change) and soil microstructure changes during the soil erosion process. They conducted a systematic study to evaluate the effect of LUCC on surface soil erosion in karst rocky desertification areas. All the previous researches have provided significant insights into the karst rocky desertification. Nevertheless, few scholars have worked on the microstructure features and changes of red clay during its loss and leakage in the karst rocky desertification area.

In this context, the objectives of this study are: (1) to identify the microstructure differences of the soil samples taken from the fields of four different land use patterns and to observe the microstructure changes of soil during its loss and leakage through MIP tests, and (2) to analyze the microstructure features of the samples taken from the fields of two different land cover patterns through SEM test, (3) to describe the relationship between the impact level of surface runoff erosion and LUCC from the microstructural perspective and to show the changing patterns of soil microstructure during its loss and leakage.

Materials and methods

Loss and leakage of red clay in karst areas

The studied area which lies in the Houzhai river basin is located in Chenqi village of Puding county, Guizhou province, China. This region has the typical karst peak cluster landform with the elevation ranging from 1338 to 1491 m. The hillsides are extremely steep and the bedrocks mostly consist of limestones and marls formed in Triassic and afterward. The red clay is widely but discontinuously spread, and the soil layer is rather thin and shallow (Fig. 1). In the last decades, the rapid population growth broke the balance between the people and land in the region. Overloaded population forced local residences to destroy forests for more farmlands. Steep slope reclamation, overgrazing, deforestation and other human activities have induced massive decline and destruction of vegetation. Furthermore, these activities have caused the changes of the physical and mechanical property of soil and accelerate the soil erosion.

In the karst areas, the surface soil and the soil leaking into cracks and caves form a dual spatial structure. This is a structure that exists only in the rocky desertification area. Generally, the dual spatial structure is formed through four steps: rainfall splash, runoff erosion, crack leakage, and underground water transportation (Fig. 2): (1) soil particles begin to break down as raindrops strike the soil surface; (2) the increased runoff turbulence induced by more raindrops will amplify the transporting ability of runoffs, which will lead to more soil loss; (3) the development of karst cracks will eventually lead to their connections to the underground cave, soil particles can flow through the cracks and finally leak into the underground; (4) the rainfall runoffs increase the underground water flow, which meanwhile increases the transportation capacity of the underground water flow. More soil particles leaking from surface will be carried and deposit along the streams.

Sample gathering

Surface runoff erosion is the key step of the soil loss and leakage. The development of it largely depends on LUCC (Wu 2004; Jiang et al. 2009). To study the influence of LUCC on soil microstructure during its loss, red clay fields of four different land use patterns (shrub grass land, burned land, slope farmland and sparse shrubs land) and two land cover patterns (with/without vegetation covers) were

Fig. 1 Surface soil accumulated in the solution groove and melting tank (note: this figure was taken by Xinbao Zhang)

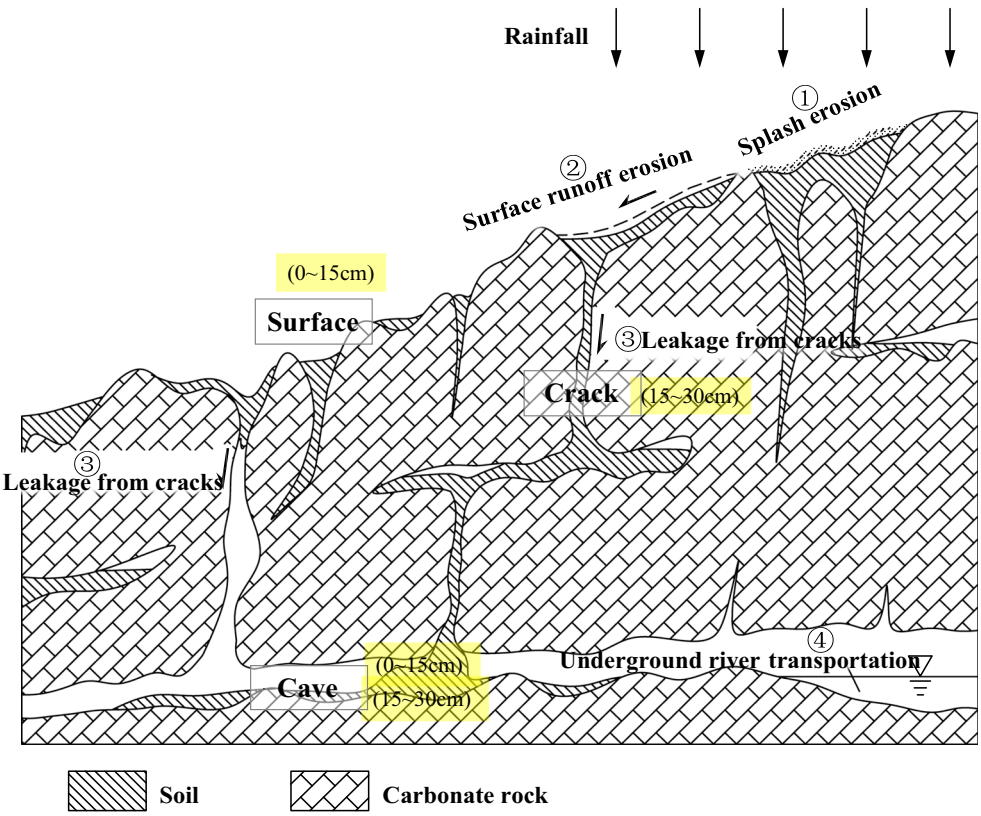

Fig. 2 Loss and leakage model of red soil in karst areas

selected as the surface runoff experimental subjects. These chosen field patterns were determined by human activities. The gathering depth ranges from the ground surface to 15 cm below.

To compare the microstructure changes of soil during its leakage, four types of soil samples were gathered from the ground surface down to the caves. The gathering depths are: 0–15 cm (surface); 15–30 cm (in the crack); 0–15 cm (in the cave); 15–30 cm (in the cave) (Fig. 2). Figure 3 shows the gathering of soil samples. Figure 3a was shot when the soil samples were gathered in the cave, and Fig. 3b was shot when the soil samples were gathered on

(a) Soil gathering in the cave (b) Soil gathering on the surface

Fig. 3 On-site soil gathering

Table 1 Basic physical property of the samples

Sample gathering	Human activities	Physical properties index				Side water content	
		Natural moisture content w/%	Natural density ρ/(g/cm^3)	Void ratio e	Specific gravity G_s	Plastic limit w_l/%	Liquid limit w_p/%
①							
Shrub grass land	Recovery after burn	44.51	1.684	1.34	2.73	23.14	41.31
Burned land	No recovery after burn	43.70	1.642	1.39	2.73	21.98	39.01
Slope farmland	Crop rotation	34.88	1.602	1.21	2.63	18.81	32.96
Sparse shrubs land	Overgrazing	36.78	1.622	1.24	2.66	19.43	35.32
②							
Surface	/	44.21	1.626	1.421	2.73	22.2	38.9
Cave	/	36.96	1.689	1.213	2.74	24.5	43.7

ground surface. Basic physical properties of the samples are shown in Table 1.

Mercury intrusion porosimetry (MIP) test

Lyophilization is a widely used and reliable method for the preparation and storage of MIP sample (Karcz et al. 2012). It can restrain the deformation of the natural pore structure of red clay to the largest extent possible during the sample drying procedure. For sample preparation, a soil bar about 1 cm^3 was cut and then placed in the liquid nitrogen for 15 min. Because the boiling point of liquid nitrogen is only −196 °C, these samples will freeze immediately. Then, these samples were installed and kept in the vacuum freeze dryer for above 20 h. Since the dryer provided a vacuum environment under −50 °C, the amorphous ice in soil samples gradually sublimated. The water vapor was discharged through the vacuum tube system. After all the samples were prepared, AutoPore IV 9500 produced by U.S. Micromeritics company was utilized to conduct the MIP test. At the beginning of the test, a soil bar was cut from the fresh fracture of the samples. Due to the restriction of the volume of dilatometer capillary (the volume decides the largest amount of intruded mercury), the sample size must satisfy: $0.25V_p < V < 0.9V_p$. V is the pore volume, V_p is the total volume of dilatometer capillary.

Scanning electron microscope (SEM) test

Scanning electron microscope S-3000 N produced by Japanese company Hitachi was applied to observe the microstructures of the samples taken from shrub grass land and burned land. This test is used to study the effect of LUCC on the soil microstructures. Lyophilization was utilized for soil sample preparation. The smooth and fresh fracture surface (must be the natural section) should be

selected for observation, so that the SEM images could be more even and clear. During the test, appropriate and typical soil units were selected to be shot from low to high magnifications for 5–7 images. To facilitate the comparison, images were zoomed to the same proportion and resolution.

Fractal dimension calculation method

Mercury porosimetry method was used to calculate the surface fractal dimension D_s of pores (Zhang and Li 1995). During the mercury intrusion, the pressure P_i and the volume of intruded mercury V_i can be related to D_s by thermodynamic relations. The surface fractal dimension D_s can be written as

$$\sum_{i=1}^{n} \overline{P_i} \cdot \Delta V_i = C' r_n^2 \left(\frac{V_n^{1/3}}{r_n} \right)^{D_s} \quad (1)$$

where $\overline{P_i}$ is the average mercury pressure for the i th time, ΔV_i is the intruded mercury volume for the ith time, r_n is pore diameter corresponding to intruded mercury for the ith time, V_n is the cumulative volume of intruded mercury when the pressure is applied for the ith time, D_s is the surface fractal dimension, C' is a constant.

If:

$$W_n = \sum_{i=1}^{n} \overline{P_i} \cdot \Delta V_i \quad (2a)$$

$$Q_n = \frac{V_n^{1/3}}{r_n} \quad (2b)$$

Substitute Formula (2a) and (2b) into Formula (1), and take the logarithm of both sides:

$$\ln\left(\frac{W_n}{r_n^2} \right) = D_s \ln Q_n + C \quad (3)$$

D_s is attained by the slope of the curve between $\ln\left(\frac{W_n}{r_n^2}\right)$ and $\ln Q_n$.

Test results and analysis

Cumulative pore volume curves

Cumulative pore volume curves (Fig. 4) can be drawn based on the results of MIP tests. These curves demonstrate the relationship between the pore diameter and its corresponding cumulative volume of the pores which have diameters equal and over this pore diameter (Bagde 2000). Due to the significant order differences of different pore diameters, the pore diameter was presented by logarithmic scale (Fig. 5). Pore volume distribution and microstructure features are shown in Table 2. Figure 5 shows that all the curves have similar shapes. Each curve contains two parts: the steep segment with pores smaller than 0.4 μm and the smooth segment with pores larger than 0.4 μm. This phenomenon indicates that the volume of the pores which are smaller than a random pore increases sharply when the diameter of this pore decreases. The pores which range from 0.01 to 0.4 μm have the largest proportion.

The differences among the curves of four land use patterns are mainly shown in the range between 0.01 and 0.4 μm (Fig. 5a). For both the curves of burned land and shrub grass land, there are steep rises between 0.01 and 0.04 μm, which presents a concave distribution in the figure. By contrast, the steep rises occur between 0.1 and 0.4 μm for the slope farmland and sparse shrubs land, which present a convex distribution. According to the curves, the soil pores for burned land and shrub grass land are predominantly micro, their diameters primarily range from 0.01 to 0.04 μm. Meanwhile, the soil pores for slope farmland and sparse shrub land are predominantly small, their diameters primarily range from 0.1 to 0.4 μm.

It can be seen that the curves of shrub grass land and burned land are on the left of the curves of slope farmland and sparse shrub land. This phenomenon illustrates that among all the four types of land, shrub grass land has the largest proportion of micro and small pores, especially the

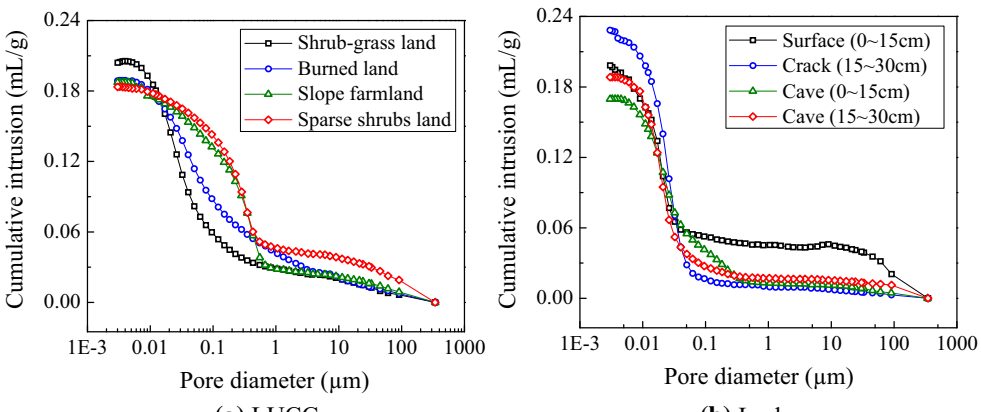

Fig. 4 Cumulative mercury intrusion curves

(a) LUCC **(b)** Leakage

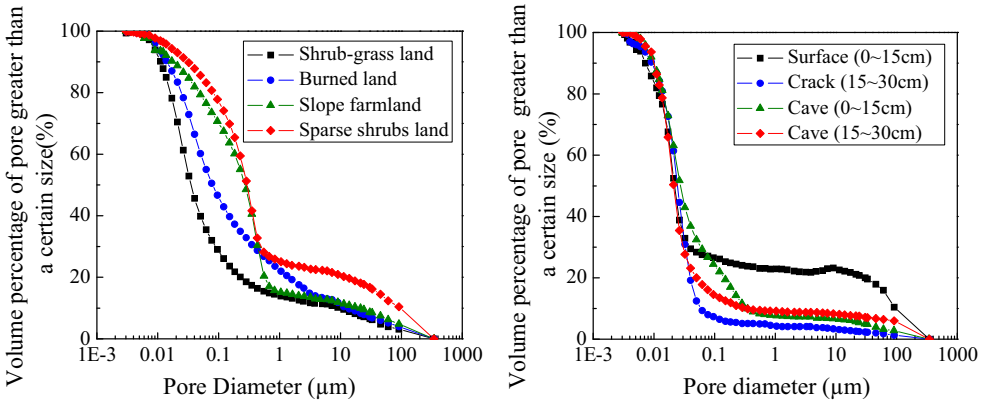

(a) LUCC **(b)** Leakage

Fig. 5 Cumulative pore volume curves

Table 2 Pore volume distribution and structure features

Sample source	Percentage of pore volume within different pore diameter, %				Total pore volume V/(mL/g)	Total specific surface area S/(m^2/g)	Average pore diameter $\bar{D}$/μm	Porosity n/%	Mercury (water) capacity coefficient R_f
	<0.04	0.04–0.4	0.4–50	>50					
①									
Shrub grass land	60.07	24.16	11.18	4.59	0.204	29.375	0.028	34.24	0.62
Burned land	39.64	36.05	11.18	5.82	0.189	18.715	0.040	32.16	0.68
Slope farmland	20.63	51.87	20.42	7.08	0.187	13.852	0.054	31.55	0.70
Sparse shrubs land	14.42	55.59	16.18	13.81	0.184	9.244	0.079	29.47	0.81
	<0.01	0.01–0.1	0.1–10	>10					
②									
Surface (0–15 cm)	16.34	57.15	4.14	22.37	0.198	45.46	17.50	32.57	0.74
Crack (15–30 cm)	11.53	81.08	4.14	3.25	0.228	50.26	18.20	37.69	0.49
Cave (0–15 cm)	10.01	76.14	5.84	8.01	0.170	29.99	22.60	30.11	0.59
Cave (15–30 cm)	12.23	64.11	17.13	6.43	0.188	39.24	19.20	32.81	0.54

micro pores. For the pore diameter over 0.4 μm, the differences of the curves are insignificant.

For the samples during leakage, the diameters of pores are predominantly distributed between 0.01 and 0.1 μm. As seen in Fig. 5b, the pore distribution differences among the samples of ground surface, cracks and caves are significant when the pore diameter is over 0.04 μm (small, medium and large pores). When the pore diameter is larger than 0.4 μm, these soil samples can be sorted by their pore volume as 'surface (0–15 cm) > cave (15–30 cm) > cave (0–15 cm) > crack (15–30 cm)'. This sequence changes to 'surface (0–15 cm) > cave (0–15 cm) > cave (15–30 cm) > crack (15–30 cm)' when the pore diameter ranges from 0.04 to 0.4 μm. It indicates that among all the samples, surface soil (0–15 cm) has the largest proportion of small, medium and large pores (pores which have diameters larger than 0.4 μm). For the soil in the cave, when the soil of shallow layers [cave (0–15 cm)] turns into deep soil [cave (15–30 cm)] through sediment and accumulation, the proportion of medium and large pores increases while the proportion of small pores decreases.

The total specific surface area of soil is mostly related to the percentages of pores in different diameter ranges. Generally, a large total specific surface area of soil indicates the proportion of small pores in the soil is also large (Anda et al. 2008). According to Table 2, even though the total pore volumes of the soil samples from four different land use patterns have insignificant differences, the total specific surface areas are significantly different. They can be sorted by their total specific surface areas as 'shrub grassland > burned land > sloping farmland > sparse shrub'. All the total specific surface areas show positive correlations with the percentages of micro and small pores which have diameters smaller than 0.4 μm. Meanwhile, they show negative correlations with the percentages of medium and large pores which have diameters larger than 0.4 μm. The result indicates that unreasonable land use

could reduce the total specific surface areas of soil and the volume of micro and small pores.

During leakage, the soil samples can be sorted by their total pore volumes as 'crack (15–30 cm) > surface (0–15 cm) > cave (15–30 cm) > cave (0–15 cm)'. The total pore volumes of all soil samples present positive correlations with the total specific surface areas, which suggest that both total pore volume and total specific surface area reduce when the soil leaks into the caves from surface. However, abnormality was noticed in the samples from crack (15–30 cm). It is because of the effect of runoff erosion. Moreover, the total volume and specific surface area of pores decrease with the increasing gathering depth of soil samples.

Pore-size distribution (PSD)

PSD curves can be obtained based on the cumulative intruded mercury curve (Fig. 6). They show the volumes of pores of different sizes (Simms and Yanful 2004). As shown in Fig. 6a, the first peaks ($\approx$0.04 μm) of shrub grass land and burned land curves are close to each other, but the peak value of burned land is obviously lower. This illustrates that vegetation burning could cause a significant reduction of micro and small pores. When the vegetation is recovered, micro and small pore volume increases significantly. The first peaks ($\approx$0.4 μm) of the slope farmland and sparse shrub land are close. The corresponding pore diameters are significantly larger than the diameters for shrub grass land and burned land. Moreover, a second peak appears between 50 and 100 μm for sparse shrubs land. It illustrates that the human activities could gradually transfer the micro pores in the soil into small pores, which eventually makes the volume of small pores predominant. Meanwhile the human activities also significantly increase the proportion of large pores in sparse shrub land.

Figure 6b shows that first peaks of all four curves appear around 0.04 μm. For the curve of surface (0–15 cm), two peaks appear in 0.04 and 80 μm, respectively. For crack (15–30 cm) and cave (0–15 cm), only a single peak exists in each curve. Although there are two peaks for the curve of cave (15–30 cm), they are very close to each other. They appear at 0.04 and 0.4 μm, respectively. It can be concluded that large pores have a larger proportion for the soil from surface (0–15 cm). Although leakage does not change the distribution range of pore diameter, the transportation and accumulation of soil in the cave certainly have an impact on the volume and characteristics of soil pores.

Fractal features of pore structure

The pore surface fractal dimension provides a way to study the complexity of pore structure quantitatively. It could reflect the physical properties of soils (Tang et al. 2013). Pore surface fractal dimension is related to the times of mercury intrusion (52 times for this test) and the volume of intruded mercury for every time. The more times of mercury intrusion could provide more data; hence, more accurate pore surface fractal dimensions (Zhang and Li 1995). Figures 7 and 8 illustrate the relationships between $\ln\left(\frac{W_n}{r_n^2}\right)$ and $\ln Q_n$. Pore surface fractal dimensions are shown in Table 3.

The samples from four different land use patterns are sorted by the pore surface fractal dimension and shown as 'shrub grass land > burned land > slope farmland > sparse shrub land'. The shrub grass land which is barely affected by human activities shows the most complex pore structure. When land cover reduces due to human activities, the pore structure of them becomes simpler. Pore surface fractal dimension reveals a positive correlation with the distribution of micro and small pores shown in

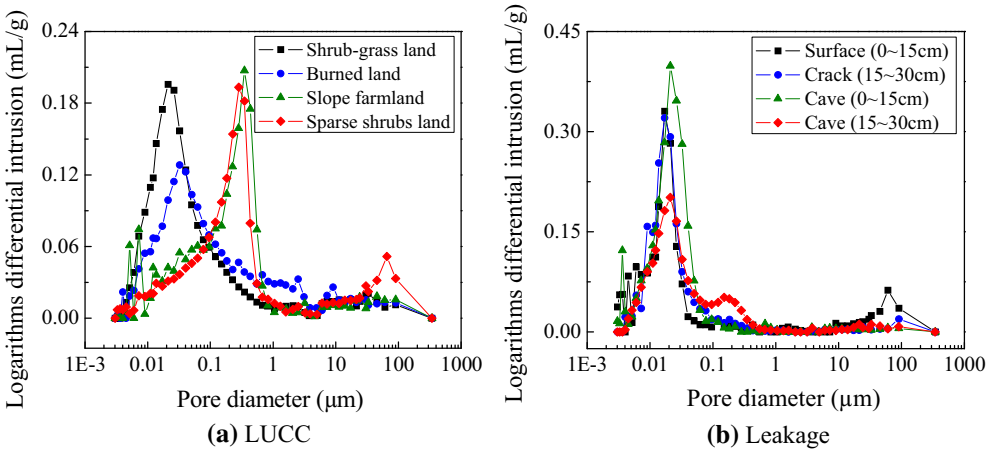

Fig. 6 Soil pore-size distribution (PSD) curves

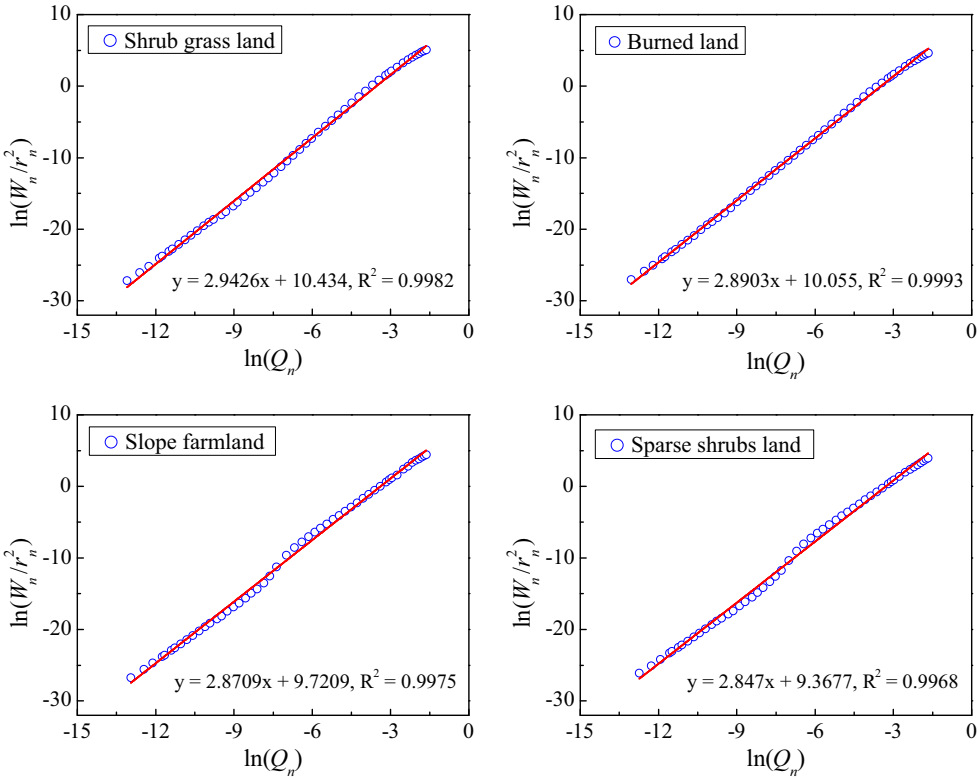

Fig. 7 Calculation on pore surface fractal dimension of the samples from four land use patterns

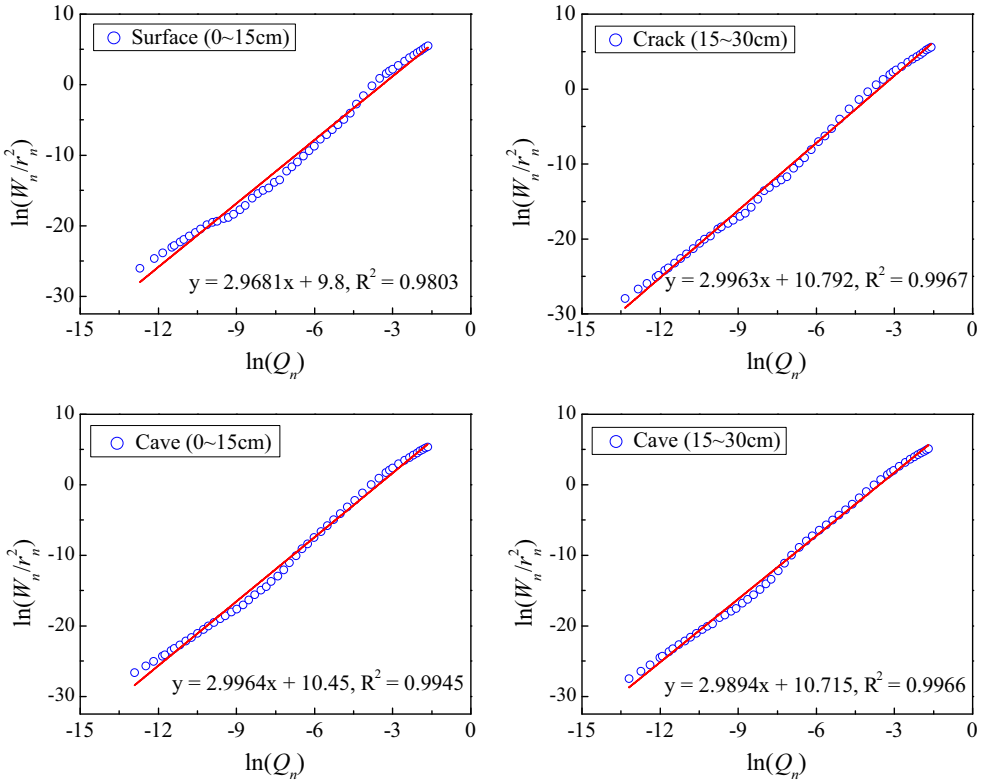

Fig. 8 Calculation on pore surface fractal dimension of the samples during leakage

Table 3 Pore surface fractal dimension

Sample gathering		Fitting formula	Fractal dimension, D_S	Decision coefficient, R^2
①	Shrub grass land	$y = 2.9426x + 10.4340$	2.9426	0.9982
	Burned land	$y = 2.8903x + 10.0550$	2.8903	0.9993
	Slope farmland	$y = 2.8709x + 9.7209$	2.8709	0.9975
	Sparse shrubs land	$y = 2.8470x + 9.3677$	2.8470	0.9968
②	Surface (0–15 cm)	$y = 2.9681x + 9.8000$	2.9681	0.9803
	Crack (15–30 cm)	$y = 2.9763x + 10.7920$	2.9763	0.9967
	Cave (0–15 cm)	$y = 2.9894x + 10.7150$	2.9894	0.9966
	Cave (15–30 cm)	$y = 2.9964x + 10.4500$	2.9964	0.9945

Fig. 5a, and this fact indicates that pore surface fractal dimension is related to the distribution of micro and small pores (<0.4 μm).

The samples during leakage are sorted by the pore surface fractal dimension and shown as 'cave (15–30 cm) > cave (0–15 cm) > crack (15–30 cm) > surface (0–15 cm)'. The pore surface fractal dimension of the sample from surface is smaller than the one from the cave. Pore surface fractal dimension reveals a negative correlation with the distribution of medium and large pores (>0.4 μm) shown in Fig. 5b. Due to the influence of vegetation root and runoff erosion, the medium and large pores increase and dominate the pore distribution of soil. Meanwhile, the proportion of micro and small pores decreases as well as the pore surface fractal dimension.

According to the analysis above, pore surface fractal dimension can reflect the pore distribution of soil. The underground soil mainly consists of micro and small particles which are eroded and transported by runoffs. After the soil particles leak into the underground, they accumulate in cracks and caves. The soil layer made of them keeps getting thicker during time. With the compaction and consolidation of the soil in the cave, the number of medium and large pores reduces significantly. Meanwhile, the proportion of micro and small pores increases. This process leads to a large surface fractal dimension (≈ 3). It also explains why the soil in the cave consists mostly of fine and sticky particles.

Scanning electron microscope images

Though the pores of different sizes exist in red clay, the micro and small pores are predominant. Compared to general clays, the void ratio of red clay is higher. The structural units of red clay are primarily comprised of irregular aggregates. During the laterization, aggregates are attached or cemented to each other by iron oxide. They turn into larger clots or flocculent structures (Rice et al. 1985; Tang et al. 2013). Pores of red clay can be divided into two main categories: intra-aggregate pores (*a* in Fig. 9) and inter-aggregate pores (*b* in Fig. 9).

As shown in Fig. 9, the aggregates of soil are in the form of clotty structure. Large amounts of pores can be seen. The mesh fibers (*c* in Fig. 9) which work like the reinforcement in civil engineering bond the soil particles together. The approximately elliptical pores of different sizes are shown in this image. The statistical analysis of the medium and large pores reveals that the major axis of the pores ranges from 11.9 to 24.7 μm and the minor axis ranges from 7.1 to 18.1 μm. Figure 10 shows that soil structure is flocculent with approximately elliptical pores of different sizes. The major axis of the pores ranges from 11 to 16 μm and the minor axis ranges from 8.4 to 11.7 μm. Compared with the SEM images of the soil taken from shrub grass land covered with vegetation, fibers such as plant roots are not found here, and the pores are smaller. This result matches the result of MIP test.

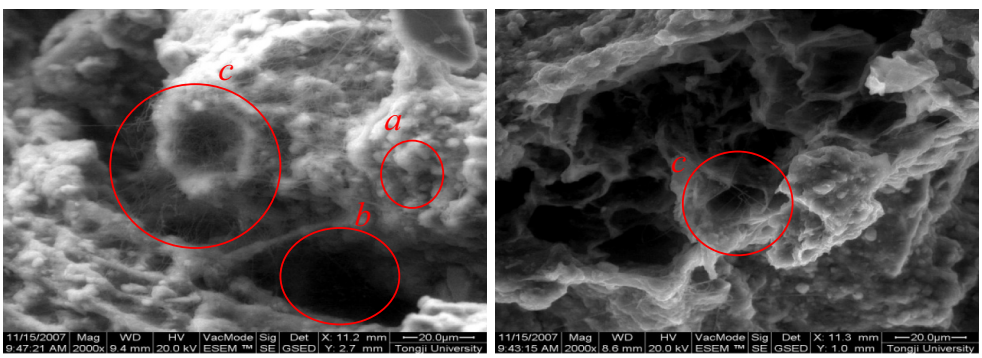

Fig. 9 Vegetation covers

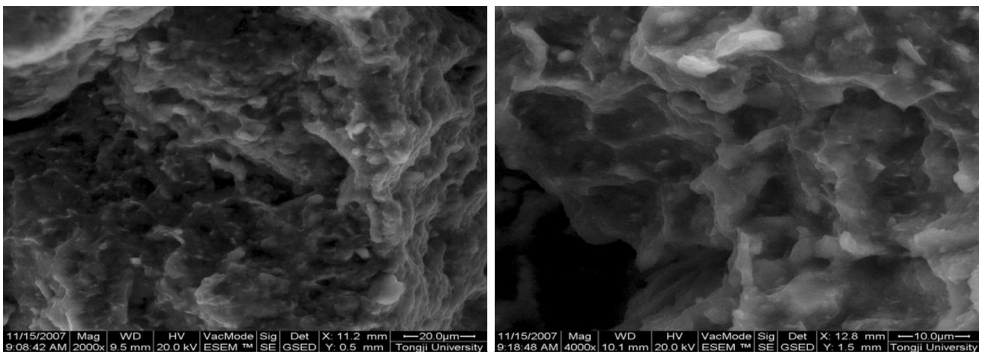

Fig. 10 No vegetation cover

Some preliminary conclusions can be obtained through SEM images. (1) The soil covered with vegetation has uniformly distributed pores. The mesh fiber in the soil can bond the particles together, which could fix the particles when they were hit by raindrops. (2) For the soil without vegetation cover, the particles cannot be bonded together without plant fibers and the pores arrange disorderly. Thus, its resistance capacity against soil erosion is weaker when hit by raindrops. It also explains why the volume of intruded mercury for the samples from the land without vegetation cover is less than the one with vegetation in MIP test.

Discussion of soil loss and leakage

Runoff erosion as a key step of loss and leakage is affected by LUCC. The impact of human activities gradually decreases from sparse shrub land to shrub grassland. The soil structure of shrub grassland contains mainly small pores, which is beneficial to the conservation of water and soil. Moreover, the vegetation roots bond the soil particles together, which enhances its resistance to the runoff erosion. Based on the data collected in the runoff experimental stations in 2008, Fig. 11 demonstrates the surface soil loss caused by rainfall in the fields of four land use patterns.

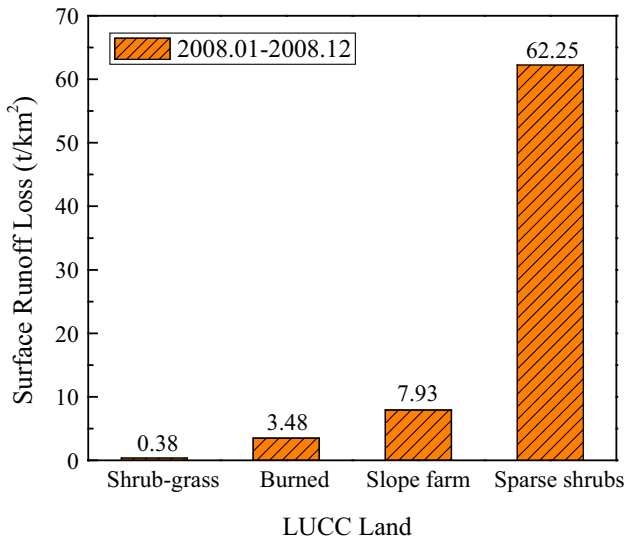

Fig. 11 Surface soil loss caused by rainfall in 2008

If the four land use patterns are sorted by their surface soil loss, the sequence is: sparse shrub land > sloping farmland > burned land > shrub grassland. According to the results of MIP test, positive correlations are revealed between the amount of surface soil loss and the proportion of medium and large pores. Meanwhile, the proportion of micro and small pores, the total pore specific surface area, and the pore surface fractal dimension all negatively correlated with the amount of surface soil loss. The results of surface soil loss clearly explain the influence of microstructure on the anti-erosion capacity of soil.

It is a dynamic process when eroded soil leaks into the underground spaces from the ground surface. When it rains, soil particles are decomposed by the impact of rain drops. The separated soil particles are transported by rain-induced runoffs. During this process, the volume of large pores increases and the surface fractal dimension of soil decreases. Then, the soil particles carried by rainfall runoff leak into the well-developed karst cracks. These particles interact with each other. They are sifted, rearranged, and eventually piled up. The soil in cracks mostly consists of fine and small particles and micro and small pores. The soil particles with medium and large pores cannot support the soil structure and leak into the caves. Although the soil accumulated in the cracks has the least medium and large pores, its total pore volume is the largest due to its loose microstructure. The soil particles leaking into the cave are carried by underground rivers. They accumulate and deposit during their transportation. Since soil from the shallow layer [cave (0–15 cm)] in the cave is constantly transported, its proportion of medium and large pores and the total pore volume are smaller compared to the soil of deep layer [cave (15–30 cm)].

The conclusions drawn here are consistent with the results obtained from MIP and SEM tests. It suggests that microstructure change of soil is related to loss and leakage process.

Conclusions

Through the field investigation, laboratory tests, and analysis, the microstructure of red clay in karst rocky desertification mountains were researched and several conclusions are drawn as follows:

(1) Among the soil samples taken from the fields of four different land use patterns, significant differences of cumulative pore volumes were observed in the micro and small size range, shrub grass land has the largest proportion. Total specific surface areas are positively correlated with the proportion of micro and small pores, and negatively correlated with the proportion of medium and large pores. Shrub grass land and burned land mainly consist of micro pores, the proportion in the former is higher. Slope farmland and sparse shrub land mainly consist of small pores, and the proportion of large pores in the latter is obviously higher. With the intensification of human activities, micro pores gradually transform into small pores.

(2) For the soil samples taken from different phases of leakage, the differences of cumulative pore volume of them lie in the range of medium to large size, and the soil sample from the surface (0–15 cm) has the largest proportion. The soil from crack (15–30 cm) has the largest total pore volume. The total pore volume and total specific surface area are positively correlated. The transportation and accumulation of soil in the cave affect pore development and its volume.

(3) The pore surface fractal dimension is negatively correlated with the impact level of human activity and it positively correlated to the distribution of micro and small pores (<0.4 μm). Pore surface fractal dimension of soil becomes larger after the soil leaks into caves.

(4) The soil aggregates of the land with vegetation cover are clotty. The mesh fibers which work like reinforcement in soil bond soil particles together.

(5) The amount of surface soil loss is positively correlated with the proportion of medium and large pores, and negatively correlated with the proportion of micro and small pores, total pore specific surface area as well as pore surface fractal dimension. These results clearly explain the influence of soil microstructure on the anti-erosion capacity of soil.

Above all, several suggestions can be concluded for the conservation of water and soil in Karst rocky-desertification region. First, the primary method to control loss and leakage of red clay is reducing the surface runoff erosion. Second, woodland reclamation, overgrazing, farming and burning should be avoided. Third, the conversion of cropland to forest is crucial for alleviating the threat of karst rocky desertification hazard and maintaining a healthy ecological system. Fourth, the formation of leakage channel in karst cracks should be restrained to reduce the leakage of red clay.

Acknowledgments This work is supported by National Key Technologies R&D Program of China (Grant No. 2012BAJ11B04), and Shanghai Leading Academic Discipline Project. Project Number: B308.

References

Anda M, Shamshuddin J, Fauziah IC, Omar SRS (2008) Pore space and specific surface area of heavy clay oxisols as affected by their mineralogy and organic matter. Soil Sci 173(8):560–574

Bagde MN (2000) An investigation into strength and porous properties of metamorphic rocks in the Himalayas: a case study. Geotech Geol Eng 18:209–219

Chen X, Zhang ZC, Chen XH, Shi P (2009) The impact of land use and land cover changes on soil moisture and hydraulic conductivity along the karst hillslopes of southwest China. Environ Earth Sci 59(4):811–820

Ellison WD (1947) Soil erosion studies. Agric Eng 28(4):15–54

Ferro ND, Berti A, Francioso O, Ferrari E, Matthews GP, Morari F (2012) Investigating the effects of wettability and pore size distribution on aggregate stability: the role of soil organic matter and the humic fraction. Eur J Soil Sci 63(2):152–164

He KQ, Jia YY, Wang B, Wang RL, Luo HL (2013) Comprehensive fuzzy evaluation model and evaluation of the karst collapse susceptibility in Zaozhuang Region. China. Natural Hazards 68(2):613–629

Hu BQ, Liao CM, Yan ZQ, Li L, Qin KX (2003) Design and application of dynamic monitoring and visualization management information system of karst land rocky desertification. Chin Geogr Sci 14(2):122–128

Huang QH, Cai YL (2007) Spatial pattern of Karst rock desertification in the middle of Guizhou province, Southwestern China. Environ Geol 52(7):1325–1330

Janža M (2010) Hydrological modeling in the karst area, Rižana spring catchment, Slovenia. Environ Earth Sci 61(5):909–920

Jiang YJ, Li LL, Groves C, Yuan DX, Kambesis (2009) Relationships between rocky desertification and spatial pattern of land use in typical karst area, Southwest China. Environ Earth Sci 59(4):881–890

Jiang ZH, Lian YQ, Qin XQ (2014) Rocky desertification in Southwest China: impacts, causes, and restoration. Earth Sci Rev 132:1–12

Karcz J, Bernas T, Nowak A, Talik E, Woznica A (2012) Application of lyophilization to prepare the nitrifying bacterial biofilm for imaging with scanning electron microscopy. Scanning 34(1):26–36

Kheir RB, Abdallah C, Khawlie M (2008) Assessing soil erosion in Mediterranean karst landscapes of Lebanon using remote sensing and GIS. Eng Geol 99(3):239–254

Li DW, Cui ZJ, Liu GN, Feng JL, Cao J (2001) Formation and evolution of karst weathering crust on limestone and its cyclic significance. Carsologica Sinica 20(3):183–188 **(in Chinese)**

Li JY, Zhu LJ, Lang F et al (2002) Study with scanning electron microscope on micro-289 texture of the residual red clay from carbonate rocks. Carsologica Sinica 21(4):233–237 **(in Chinese)**

Осипов ВИ (1985) Essence of strength and deformation properties of clay type and rocks. Geological Publishing House, Beijing, pp 15–39 **(in Chinese)**

Olson TC, Wischmeier WH (1963) Soil-erodibility evaluations for soils on the runoff and erosion stations. Soil Sci Soc Am J 27(5):590–592

Rice TJ, Weed SB, Buol SW (1985) Soil-saprolite Profiles Derived from Mafic Pocksin the North Carolina Piedmont: II.Association of Free Iron Oxides with Soil and Clay. Soil Sci Soc Am J 49:178–185

Simms PH, Yanful EK (2004) A discussion of the application of mercury intrusion porosimetry for the investigation of soils, including an evaluation of its use to estimate volume change in compacted clayey soils. Géotechnique 54(6):421–426

Tang YQ, She TY, Zhang XH et al (2009) Changing of red clay shear strength with water content under rainfall in karst rocky desertification areas, Guizhou province. J Eng Geol 17(2):249–252 **(in Chinese)**

Tang YQ, Zhang XH, Zhou J et al (2010) The mechanism of underground leakage of soil in karst rocky desertification areas—A case in Chenqi small water, Puding, Guizhou province. Carsologica Sinica 29(2):121–127 **(in Chinese)**

Tang YQ, Li J, Zhang XH et al (2013) Fractal features and stability of soil aggregates in karst rocky desertification areas. Nat Hazards 65:563–579

Terzaghi K, Peck RB, Mesri G (1996) Soil mechanics in engineering practice. Wiley, New York, pp 10–70

Tobias HK, Julie D, Simon JB, John BT, David WH, Rudy S (2012) Sedimentology 59(2):623–645

Trudgill ST, Clayton KM (1985) Limestone geomorphology. Longman, New York, pp 9–40

Wang WB (2008) Study on LUCC and soil erosion of small catchment in karst area. Beijing university (**in Chinese**)

Wang SJ, Liu QM, Zhang DF (2004) Karst rocky desertification in southwestern China: geomorphology, land use, impact and rehabilitation. Land Degrad 15(2):115–121

Wang JX, Zhou BP, Liu Y, Tang YQ, Zhang XB, Yang P (2014) Erosion-creep-collapse mechanism of underground soil loss for the karst rocky desertification in Chenqi village, Puding county, Guizhou, China. Environ Earth Sci 72(8):2751–2764

Wu XQ (2004) Effects of land use/land cover changes on soil erosion—a case study of a small karst catchment in southwestern China. Beijing University (**in Chinese**)

Xiong YJ, Qiu GY, Mo DK, Lin H, Sun H, Wang QX, Zhao SH, Yin J (2009) Rocky desertification and its causes in karst areas: a case study in Yongshun County, Hunan province, China. Environ Geol 57(7):1481–1488

Yang P, Tang YQ, Zhou NQ, Wang JX, She TY, Zhang XH (2011) Characteristics of red clay creep in karst caves and loss leakage of soil in the karst rocky desertification area of Puding County, Guizhou, China. Environ Earth Sci 63(3):543–549

Yang QY, Jiang ZC, Ma ZL, Luo WQ, Xie YQ, Cao JH (2013) Relationship between karst rocky desertification and its distance to roadways in a typical karst area of Southwest China. Environ Earth Sci 70(1):295–302

Yang QY, Jiang ZC, Yuan DX, Ma ZL, Xie YQ (2014) Temporal and spatial changes of karst rocky desertification in ecological reconstruction region of Southwest China. Environ Earth Sci 72(11):4483–4489

Yuan DX (1996) Southwest karst mountain environmental geological problems in our country. Explor Nat 15(58):21–23 **(in Chinese)**

Zhang BQ, Li SF (1995) Determination of the surface fractal dimension for porous media by mercury porosimetry. Ind Eng Chem Res 34:1383–1386

Zhou J, Tang YQ, Zhang XH, She TY, Yang P, Wang JX (2012) The influence of water content on soil erosion in the desertification area of Guizhou, China. Carbonates Evaporites 27(2):185–192